
Direct Diffusion Bridge using Data Consistency for Inverse Problems

Hyungjin Chung¹ Jeongsol Kim¹ Jong Chul Ye²

¹Dept. of Bio and Brain Engineering

²Graduate School of AI

Korea Advanced Institute of Science and Technology (KAIST)

{hj.chung, jeongsol, jong.ye}@kaist.ac.kr

Abstract

Diffusion model-based inverse problem solvers have shown impressive performance, but are limited in speed, mostly as they require reverse diffusion sampling starting from noise. Several recent works have tried to alleviate this problem by building a diffusion process, directly bridging the clean and the corrupted for specific inverse problems. In this paper, we first unify these existing works under the name Direct Diffusion Bridges (DDB), showing that while motivated by different theories, the resulting algorithms only differ in the choice of parameters. Then, we highlight a critical limitation of the current DDB framework, namely that it does not ensure data consistency. To address this problem, we propose a modified inference procedure that imposes data consistency without the need for fine-tuning. We term the resulting method data Consistent DDB (CDDB), which outperforms its inconsistent counterpart in terms of both perception and distortion metrics, thereby effectively pushing the Pareto-frontier toward the optimum. Our proposed method achieves state-of-the-art results on both evaluation criteria, showcasing its superiority over existing methods. Code is open-sourced at <https://github.com/HJ-harry/CDDB>

1 Introduction

Diffusion models [15, 38] have become the de facto standard of recent vision foundation models [32, 31, 33]. Among their capabilities is the use of diffusion models as generative priors that can serve as plug-and-play building blocks for solving inverse problems in imaging [18, 38, 21, 5]. Diffusion model-based inverse problem solvers (DIS) have shown remarkable performance and versatility, as one can leverage the powerful generative prior regardless of the given problem at hand, scaling to linear [18, 38, 21], non-linear [5, 36], and noisy problems [21, 5].

Although there are many advantages of DIS, one natural limitation is its slow inference. Namely, the overall process of inference—starting from Gaussian noise and being repeatedly denoised to form a clean image—is kept the same, although there are marginal changes made to keep the sampling process consistent with respect to the given measurement. In such cases, the distance between the reference Gaussian distribution and the data distribution remains large, requiring inevitably a large number of sampling steps to achieve superior sample quality. On the other hand, the distribution of the measurements is much more closely related to the distribution of the clean images. Thus, intuitively, it would cost us much less compute if we were allowed to start the sampling process directly from the measurement, as in the usual method of direct inversion in supervised learning schemes.

Interestingly, several recent works aimed to tackle this problem under several different theoretical motivations: 1) Schrödinger bridge with paired data [26], 2) a new formulation of the diffusion process

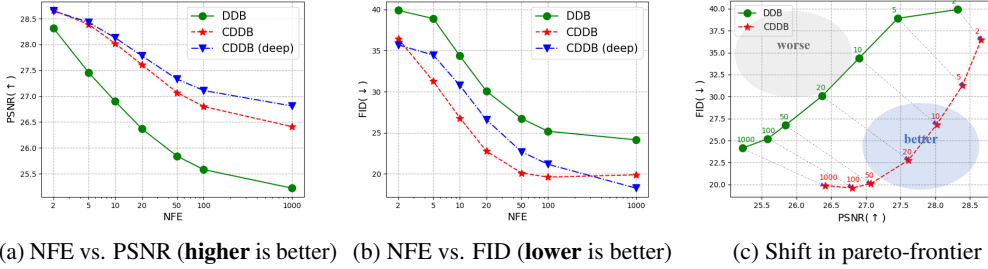


Figure 1: Quantitative metric of I^2SB [26] (denoted DDB) vs. proposed CDDB on sr4x-bicubic task.

via constant-speed continual degradation [9], and 3) Ornstein-Uhlenbeck stochastic differential equation (OU-SDE) [28]. While developed from distinct motivations, the resulting algorithms can be understood in a unifying framework with minor variations: we define this new class of methods as **Direct Diffusion Bridges** (DDB; Section 3.1). In essence, DDB defines the diffusion process from the clean image distribution in $t = 0$ to the measurement distribution in $t = 1$ as the convex combination between the paired data, such that the samples \mathbf{x}_t goes through continual degradation as $t = 0 \rightarrow 1$. In training, one trains a time-conditional neural network G_θ that learns a mapping to \mathbf{x}_0 for all timesteps, resulting in an iterative sampling procedure that *reverts* the measurement process.

Using such an iterative sampling process, one can flexibly choose the number of neural function evaluations (NFE) to generate reconstructions that meet the desiderata: with low NFE, less distortion can be achieved as the reconstruction regresses towards the mean [9]; with high NFE, one can opt for high perceptual quality at the expense of some distortion from the ground truth. This intriguing property of DDB creates a Pareto-frontier of reconstruction quality, where our desire would be to maximally pull the plot towards high perception and low distortion (bottom right corner of Fig. 1c).

In this work, we assert that DDB is missing a crucial component of *data consistency*, and devise methods to make the models *consistent* with respect to the given measurement by only modifying the sampling algorithm, without any fine-tuning of the pre-trained model. We refer to this new class of models as data **C**onsistent **D**irect **D**iffusion **B**ridge (CDDB; Section 3.2), and show that CDDB is capable of pushing the Pareto-frontier further towards the optima (lower distortion: Fig. 1a, higher perception: Fig. 1b, overall trend: Fig. 1c) across a variety of tasks. Theoretically, we show that CDDB is a generalization of DDS (Decomposed Diffusion Sampling) [6], a recently proposed method tailored for DIS with Gaussian diffusion, which guarantees stable and fast sampling. We then propose another variation, CDDB-deep, which can be derived as the DDB analogue of the DPS [5] by considering *deeper* gradients, which even further boosts the performance for certain tasks and enables the application to nonlinear problems where one cannot compute gradients in the usual manner (e.g. JPEG restoration). In the experiments, we showcase the strengths of each algorithm and show how one can flexibly construct and leverage the algorithms depending on the circumstances.

2 Background

2.1 Diffusion models

Diffusion models [15, 38, 22, 19] defines the forward data noising process $p(\mathbf{x}_t|\mathbf{x}_0)$ as

$$\mathbf{x}_t = \alpha_t \mathbf{x}_0 + \sigma_t \mathbf{z}, \mathbf{z} \sim \mathcal{N}(0, \mathbf{I}) \text{ for } t \in [0, 1], \quad (1)$$

where α_t, σ_t controls the signal component and the noise component, respectively, and are usually designed such that $\alpha_t^2 + \sigma_t^2 = 1$ [15, 22]. Starting from the data distribution $p_{\text{data}} := p(\mathbf{x}_0)$, the noising process in (1) gradually maps $p(\mathbf{x}_t)$ towards isotropic Gaussian distribution as $t \rightarrow 1$, i.e. $p(\mathbf{x}_1) \simeq \mathcal{N}(0, \mathbf{I})$. Training a neural network to *reverse* the process amounts to training a residual denoiser

$$\min_{\theta} \mathbb{E}_{\mathbf{x}_t \sim p(\mathbf{x}_t|\mathbf{x}_0), \mathbf{x}_0 \sim p_{\text{data}}(\mathbf{x}_0), \epsilon \sim \mathcal{N}(0, \mathbf{I})} \left[\|\epsilon_\theta^{(t)}(\mathbf{x}_t) - \epsilon\|_2^2 \right], \quad (2)$$

such that $\epsilon_{\theta^*}^{(t)}(\mathbf{x}_t) \simeq \frac{\mathbf{x}_t - \alpha_t \mathbf{x}_0}{\sigma_t}$. Furthermore, it can be shown that epsilon matching is equivalent to the denoising score matching (DSM) [16, 37] objective up to a constant with different parameterization

$$\min_{\theta} \mathbb{E}_{\mathbf{x}_t, \mathbf{x}_0, \epsilon} \left[\|\mathbf{s}_{\theta}^{(t)}(\mathbf{x}_t) - \nabla_{\mathbf{x}_t} \log p(\mathbf{x}_t | \mathbf{x}_0)\|_2^2 \right], \quad (3)$$

such that $\mathbf{s}_{\theta^*}^{(t)}(\mathbf{x}_t) \simeq -\frac{\mathbf{x}_t - \alpha_t \mathbf{x}_0}{\sigma_t^2} = -\epsilon_{\theta^*}^{(t)}(\mathbf{x}_t)/\sigma_t$. Moreover, for optimal θ^* and under regularity conditions, $\mathbf{s}_{\theta^*}(\mathbf{x}_t) = \nabla_{\mathbf{x}_t} \log p(\mathbf{x}_t)$. Then, sampling from the distribution can be performed by solving the reverse-time generative SDE/ODE [38, 19] governed by the score function. It is also worth mentioning that the posterior mean, or the so-called denoised estimate can be computed via Tweedie’s formula [13]

$$\hat{\mathbf{x}}_{0|t} := \mathbb{E}_{p(\mathbf{x}_0 | \mathbf{x}_t)}[\mathbf{x}_0 | \mathbf{x}_t] = \frac{1}{\alpha_t} (\mathbf{x}_t + \sigma_t^2 \nabla_{\mathbf{x}_t} \log p(\mathbf{x}_t)) \simeq \frac{1}{\alpha_t} (\mathbf{x}_t + \sigma_t^2 \mathbf{s}_{\theta^*}^{(t)}(\mathbf{x}_t)). \quad (4)$$

In practice, DDPM/DDIM solvers [15, 35] work by iteratively refining these denoised estimates.

2.2 Diffusion model-based inverse problem solving with gradient guidance

Suppose now that we are given a measurement \mathbf{y} obtained through some Gaussian linear measurement process \mathbf{A} , where our goal is to sample from the posterior distribution $p(\mathbf{x} | \mathbf{y})$. Starting from the sampling process of running the reverse SDE/ODE to sample from the prior distribution, one can modify the score function to adapt it for posterior sampling [38, 5]. By Bayes rule, $\nabla_{\mathbf{x}_t} \log p(\mathbf{x}_t | \mathbf{y}) = \nabla_{\mathbf{x}_t} \log p(\mathbf{x}_t) + \nabla_{\mathbf{x}_t} \log p(\mathbf{y} | \mathbf{x}_t)$, where $\nabla_{\mathbf{x}_t} \log p(\mathbf{x}_t) \simeq \mathbf{s}_{\theta^*}(\mathbf{x}_t)$. However, $\nabla_{\mathbf{x}_t} \log p(\mathbf{y} | \mathbf{x}_t)$ is intractable. Several methods have been proposed to approximate this time-dependent likelihood, two of the most widely used being DPS [5] and Π GDM [36]. DPS proposes the following Jensen approximation¹

$$\nabla_{\mathbf{x}_t} \log p(\mathbf{y} | \mathbf{x}_t) \stackrel{(\text{DPS})}{\simeq} \nabla_{\mathbf{x}_t} \log p(\mathbf{y} | \hat{\mathbf{x}}_{0|t}) = \frac{\partial \hat{\mathbf{x}}_{0|t}}{\partial \mathbf{x}_t} \frac{\partial \|\mathbf{A} \hat{\mathbf{x}}_{0|t} - \mathbf{y}\|_2^2}{\partial \hat{\mathbf{x}}_{0|t}} = \underbrace{\frac{\partial \hat{\mathbf{x}}_{0|t}}{\partial \mathbf{x}_t}}_{\mathbf{J}} \underbrace{\mathbf{A}^\top (\mathbf{y} - \mathbf{A} \hat{\mathbf{x}}_{0|t})}_{\mathbf{V}}, \quad (5)$$

of which the chain rule is based on the denominator layout notation [41]. Here, we see that the gradient term can be represented as the Jacobian (J) vector (V) product (JVP). In the original implementation of DPS, the two terms are not computed separately, but computed directly as $\nabla_{\mathbf{x}_t} \|\mathbf{y} - \mathbf{A} \hat{\mathbf{x}}_{0|t}\|_2^2$, where the whole term can be handled with backpropagation. By this choice, DPS can also handle non-linear operators when the gradients can be computed, e.g. phase retrieval, forward model given as a neural network. On the other hand, Π GDM proposes

$$\nabla_{\mathbf{x}_t} \log p(\mathbf{y} | \mathbf{x}_t) \stackrel{(\Pi\text{GDM})}{\simeq} \mathcal{N}(\mathbf{A} \hat{\mathbf{x}}_{0|t}, \mathbf{A} \mathbf{A}^\top + \mathbf{I}) = \underbrace{\frac{\partial \hat{\mathbf{x}}_{0|t}}{\partial \mathbf{x}_t}}_{\mathbf{J}} \underbrace{\mathbf{A}^\dagger (\mathbf{y} - \mathbf{A} \hat{\mathbf{x}}_{0|t})}_{\mathbf{V}}, \quad (6)$$

where $\mathbf{A}^\dagger := \mathbf{A}^\top (\mathbf{A} \mathbf{A}^\top)^{-1}$ is the Moore-Penrose pseudo-inverse. Using the JVP for implementation, it is no longer required that the whole term is differentiable. For this reason, Π GDM can be applied to cases where we have non-differentiable, non-linear measurements given that an operation analogous to pseudo-inverse can be derived, e.g. JPEG restoration. Notably, the update step of DPS can be achieved by simply pre-conditioning Π GDM with $\mathbf{A}^\top \mathbf{A}$. Implementing DIS with DPS (5) or Π GDM (6) amounts to augmenting the gradient descent steps in between the ancestral sampling iterations.

While these methods are effective and outperforms the prior projection-based approaches [38, 21], they also have several drawbacks. Namely, the incorporation of the U-Net Jacobian is slow, compute-heavy, and often unstable [12, 34]. For example, when applied to MRI reconstruction in medical imaging, DPS results in noisy reconstructions [6] possibly due to unstable incorporation of the Wirtinger derivatives [23], and Π GDM is hard to use as it is non-trivial to compute \mathbf{A}^\dagger . In order to circumvent these issues, DDS [6] proposed to use numerical optimization (i.e. conjugate gradients; CG) in the clean image domain, bypassing the need to compute J. Consequently, DDS achieves fast and stable reconstructions for inverse problems in medical imaging.

	I ² SB [26]	InDI [9]
Definition		
Motivation	Schrödinger bridge	Small-step MMSE
Base process	$\beta_t = \begin{cases} \beta_{\min} + 2\beta_d t, & t \in [0, 0.5) \\ 2\beta_{\max} - 2\beta_d t, & t \in [0.5, 1.0] \end{cases}$	-
	$\gamma_t = \int_0^t \beta_\tau d\tau, \bar{\gamma}_t = \int_t^1 \beta_\tau d\tau$	-
	Linear symmetric	Const
Diffusion process		
α_t	$\gamma_t^2 / (\gamma_t^2 + \bar{\gamma}_t^2)$	t
σ_t^2	$\gamma_t^2 \bar{\gamma}_t^2 / (\gamma_t^2 + \bar{\gamma}_t^2)$	$t^2 \epsilon_t^2$
Sampling		
$\alpha_{s t}^2$	γ_s^2 / γ_t^2	s/t
$\sigma_{s t}^2$	$\frac{(\gamma_t^2 - \gamma_s^2) \gamma_s^2}{\gamma_t^2}$	$s^2(\epsilon_s^2 - \epsilon_t^2)$

Table 1: Comparison between different types of DDB. $\beta_d := \beta_{\max} - \beta_{\min}$. Further details are given in Appendix B.

3 Main Contributions

3.1 Direct Diffusion Bridge

We consider the case where we can sample $\mathbf{x}_0 := \mathbf{x} \sim p(\mathbf{x})$, and $\mathbf{x}_1 := \mathbf{y} \sim p(\mathbf{y}|\mathbf{x})^2$, i.e. paired data for training. Adopting the formulation of I²SB [26] we define the posterior of \mathbf{x}_t to be the product of Gaussians $\mathcal{N}(\mathbf{x}_t; \mathbf{x}_0, \gamma_t^2)$ and $\mathcal{N}(\mathbf{x}_t; \mathbf{x}_1, \bar{\gamma}_t^2)$, such that

$$p(\mathbf{x}_t | \mathbf{x}_0, \mathbf{x}_1) = \mathcal{N}\left(\mathbf{x}_t; \frac{\bar{\gamma}_t^2}{\gamma_t^2 + \bar{\gamma}_t^2} \mathbf{x}_0 + \frac{\gamma_t^2}{\gamma_t^2 + \bar{\gamma}_t^2} \mathbf{x}_1, \frac{\gamma_t^2 \bar{\gamma}_t^2}{\gamma_t^2 + \bar{\gamma}_t^2} \mathbf{I}\right). \quad (7)$$

Note that the sampling of \mathbf{x}_t from (7) can be done by the reparametrization trick

$$\mathbf{x}_t = (1 - \alpha_t) \mathbf{x}_0 + \alpha_t \mathbf{x}_1 + \sigma_t \mathbf{z}, \quad \mathbf{z} \sim \mathcal{N}(0, \mathbf{I}), \quad (8)$$

where $\alpha_t := \frac{\gamma_t^2}{\gamma_t^2 + \bar{\gamma}_t^2}$, $\sigma_t^2 := \frac{\gamma_t^2 \bar{\gamma}_t^2}{\gamma_t^2 + \bar{\gamma}_t^2}$. This diffusion bridge introduces a *continual* degradation process by taking a convex combination of $(\mathbf{x}_0, \mathbf{x}_1)$, starting from the clean image at $t = 0$ to maximal degradation at $t = 1$, with additional stochasticity induced by the noise component σ_t . Our goal is to train a time-dependent neural network that maps any \mathbf{x}_t to \mathbf{x}_0 that recovers the clean image. The training objective for I²SB [26] analogous to denoising score matching (DSM) [16] reads

$$\min_{\theta} \mathbb{E}_{\mathbf{y} \sim p(\mathbf{y}|\mathbf{x}), \mathbf{x} \sim p(\mathbf{x}), t \sim U(0,1)} \left[\left\| \mathbf{s}_{\theta}(\mathbf{x}_t) - \frac{\mathbf{x}_t - \mathbf{x}_0}{\gamma_t} \right\|_2^2 \right], \quad (9)$$

which is also equivalent to training a residual network G_{θ} with $\min_{\theta} \mathbb{E}[\|G_{\theta}(\mathbf{x}_t) - \mathbf{x}_0\|_2^2]$. For brevity, we simply denote the trained networks as G_{θ^*} even if it is parametrized otherwise. Once the network is trained, we can reconstruct \mathbf{x}_0 starting from \mathbf{x}_1 by, for example, using DDPM ancestral sampling [15], where the posterior for $s < t$ reads

$$p(\mathbf{x}_s | \mathbf{x}_0, \mathbf{x}_t) = \mathcal{N}(\mathbf{x}_s; (1 - \alpha_{s|t}^2) \mathbf{x}_0 + \alpha_{s|t}^2 \mathbf{x}_t, \sigma_{s|t}^2 \mathbf{I}), \quad (10)$$

with $\alpha_{s|t}^2 := \frac{\gamma_s^2}{\gamma_t^2}$, $\sigma_{s|t}^2 := \frac{(\gamma_t^2 - \gamma_s^2) \gamma_s^2}{\gamma_t^2}$. At inference, \mathbf{x}_0 is replaced with a neural network-estimated $\hat{\mathbf{x}}_{0|t}$ to yield $\mathbf{x}_s \sim p(\mathbf{x}_s | \hat{\mathbf{x}}_{0|t}, \mathbf{x}_t)$.

However, when the motivation is to introduce 1) a tractable training objective that learns to recover the clean image along the degradation trajectory, and 2) devise a sampling method to gradually revert the degradation process, we find that the choices made for the parameters in (8),(7) can be arbitrary, as long as the marginal can be retrieved in the sampling process (10). In Table 1, we summarize the

¹We ignore scaling constants that are related to the measurement noise for simplicity. For implementation, this can be absorbed into the choice of step sizes.

²For cases where there is a dimensionality mismatch, we use $\mathbf{x}_1 = \mathbf{A}^{\dagger} \mathbf{y}$. We keep this notation for simplicity.

³Hereafter, we override the definition of signal, noise coefficients α_t, σ_t that was first defined in Eq. (1).

Algorithm 1 CDDB

Require: $G_{\theta^*}, \mathbf{x}_1, \alpha_i, \sigma_i, \alpha_{i-1|i}^2, \sigma_{i-1|i}^2, \rho_i$
1: **for** $i = N - 1$ to 0 **do**
2: $\hat{\mathbf{x}}_{0|i} \leftarrow G_{\theta^*}(\mathbf{x}_i)$
3: $\mathbf{z} \sim \mathcal{N}(\mathbf{0}, \mathbf{I})$
4: $\mathbf{x}'_{i-1} \leftarrow (1 - \alpha_{i-1|i}^2)\hat{\mathbf{x}}_{0|i}$
 $\quad + \alpha_{i-1|i}^2\mathbf{x}_i + \sigma_{i-1|i}\mathbf{z}$
5: $\mathbf{g} \leftarrow \mathbf{A}^\top(\mathbf{y} - \mathbf{A}\hat{\mathbf{x}}_{0|i})$
6: $\mathbf{x}_{i-1} \leftarrow \mathbf{x}'_{i-1} + \rho_{i-1}\mathbf{g}$
7: **end for**
8: **return** \mathbf{x}_0

Algorithm 2 CDDB (deep)

Require: $G_{\theta^*}, \mathbf{x}_1, \alpha_i, \sigma_i, \alpha_{i-1|i}^2, \sigma_{i-1|i}^2, \rho_i$
1: **for** $i = N - 1$ to 0 **do**
2: $\hat{\mathbf{x}}_{0|i} \leftarrow G_{\theta^*}(\mathbf{x}_i)$
3: $\mathbf{z} \sim \mathcal{N}(\mathbf{0}, \mathbf{I})$
4: $\mathbf{x}'_{i-1} \leftarrow (1 - \alpha_{i-1|i}^2)\hat{\mathbf{x}}_{0|i}$
 $\quad + \alpha_{i-1|i}^2\mathbf{x}_i + \sigma_{i-1|i}\mathbf{z}$
5: $\mathbf{g} \leftarrow \frac{\partial \hat{\mathbf{x}}_{0|i}}{\partial \mathbf{x}_i} \mathbf{A}^\top(\mathbf{y} - \mathbf{A}\hat{\mathbf{x}}_{0|i})$
6: $\mathbf{x}_{i-1} \leftarrow \mathbf{x}'_{i-1} + \rho_{i-1}\mathbf{g}$
7: **end for**
8: **return** \mathbf{x}_0

choices made in [9, 26] to emphasize that the difference stems mostly from the parameter choices and not something fundamental. Concretely, sampling \mathbf{x}_t from paired data can always be represented as (8): a convex combination of \mathbf{x}_0 and \mathbf{x}_1 with some additional noise. Reverse diffusion at inference can be represented as (10): a convex combination of \mathbf{x}_0 and \mathbf{x}_t with some stochasticity. We define the methods that belong to this category as Direct Diffusion Bridge (DDB) henceforth. Below, we formally state the equivalence between the algorithms, with proofs given in Appendix A.

Theorem 1. *Let the parameters of InDI [9] in Table 1 be $t := \frac{\gamma_t^2}{\gamma_t^2 + \bar{\gamma}_t^2}$, $\epsilon_t^2 := \frac{\bar{\gamma}_t^2}{\gamma_t^2}(\gamma_t^2 + \bar{\gamma}_t^2)$. Then, InDI and I^2SB are equivalent.*

The equivalence relation will be useful when we derive our CDDB algorithm in Section 3.2. As a final note, IR-SDE [28] does not strictly fall into this category as the sampling process is derived from running the reverse SDE. However, the diffusion process can still be represented as (8) by setting $\alpha_t = 1 - e^{-\bar{\theta}t}$, $\sigma_t^2 = \lambda^2(1 - e^{-2\bar{\theta}t})$, and the only difference comes from the sampling procedure.

3.2 Data Consistent Direct Diffusion Bridge

Motivation Regardless of the choice in constructing DDB, there is a crucial component that is missing from the framework. While the sampling process (10) starts directly from the measurement (or equivalent), as the predictions $\hat{\mathbf{x}}_{0|t} = G_\theta(\mathbf{x}_t)$ are imperfect and are never guaranteed to preserve the measurement condition $\mathbf{y} = \mathbf{A}\mathbf{x}$, the trajectory can easily deviate from the desired path, while the residual blows up. Consequently, this may result in inferior sample quality, especially in terms of distortion. In order to mitigate this downside, our strategy is to keep the DDB sampling strategy (10) intact and augment the steps to constantly *guide* the trajectory to satisfy the data consistency, similar in spirit to gradient guidance in DIS. Here, we focus on the fact that the clean image estimates $\hat{\mathbf{x}}_{0|t}$ is produced at every iteration, which can be used to compute the residual with respect to the measurement \mathbf{y} . Taking a gradient step that minimizes this residual after every sampling step results in Algorithm 1, which we name data Consistent DDB (CDDB). In the following, we elaborate on how the proposed method generalizes DDS which was developed for DIS.

CDDB as a generalization of DDS [6] Rewriting (10) with reparameterization trick

$$\mathbf{x}_s = \underbrace{\hat{\mathbf{x}}_{0|t}}_{\text{Denoise}(\mathbf{x}_t)} + \underbrace{\alpha_{s|t}^2(\mathbf{x}_t - \hat{\mathbf{x}}_{0|t})}_{\text{Noise}(\mathbf{x}_t)} + \sigma_{s|t}\mathbf{z}, \quad \hat{\mathbf{x}}_{0|t} := G_{\theta^*}(\mathbf{x}_t) \quad (11)$$

we see that the iteration decomposes into three terms: the denoised component, the deterministic noise, and the stochastic noise. The key observation of DDIM [35] is that if the score network is fully expressive, then the deterministic noise term $\mathbf{x}_t - \hat{\mathbf{x}}_{0|t}$ becomes Gaussian such that it satisfies the total variance condition

$$\left(\alpha_{s|t}^2\sigma_t\right)^2 + \sigma_{s|t}^2 = \sigma_s^2, \quad (12)$$

allowing (11) to restore the correct marginal $\mathcal{N}(\mathbf{x}_s; \mathbf{x}_0, \sigma_s^2)$. Under this condition, DDS showed that using a few step of numerical optimization ensure the updates from the denoised image $\hat{\mathbf{x}}_{0|t}$ remain on the clean manifold. Furthermore, subsequent noising process using deterministic and stochastic noises can then be used to ensure the transition to the correct noisy manifold [6].

Under this view, our algorithm can be written concisely as

$$\mathbf{x}_s \leftarrow \underbrace{\hat{\mathbf{x}}_{0|t} + \rho \mathbf{A}^\top (\mathbf{y} - \mathbf{A} \hat{\mathbf{x}}_{0|t})}_{\text{CDenoise}(\mathbf{x}_t)} + \underbrace{\alpha_{s|t}^2 (\mathbf{x}_t - \hat{\mathbf{x}}_{0|t})}_{\text{Noise}(\mathbf{x}_t)} + \sigma_{s|t} \mathbf{z}, \quad (13)$$

where we make the update step only to the clean denoised component, and leave the other components as is. In order to achieve proper sampling that obeys the marginals, it is important to show that the remaining components constitute the correct noise variance and the condition assuming Gaussianity should be (12). In the following, we show that this is indeed satisfied for the two cases of direction diffusion bridge (DDB):

Theorem 2. *The total variance condition (12) is satisfied for both I²SB and InDI.*

Proof. For InDI, considering the noise variance $\sigma_t = t\epsilon_t$ in Table 1,

$$\left(\alpha_{s|t}^2 \sigma_t\right)^2 + \sigma_{s|t}^2 = \frac{s^2}{t^2} t^2 \epsilon_t^2 + s^2 (\epsilon_s^2 - \epsilon_t^2) = s^2 \epsilon_s^2 = \sigma_s^2. \quad (14)$$

Due to the equivalence in Theorem 1, the condition is automatically satisfied in I²SB. We show that this is indeed the case in Appendix A. \square

In other words, given that the gradient descent update step in $\text{CDenoise}(\mathbf{x}_t)$ does not leave the clean data manifold, it is guaranteed that the intermediate samples generated by (13) will stay on the correct noisy manifold [6]. In this regard, CDDDB can be thought of as the DDB-generalized version of DDS. Similar to DDS, CDDDB does not require the computation of heavy U-Net Jacobians and hence introduces negligible computation cost to the inference procedure, while being robust in the choice of step size.

CDDDB-deep As shown in DPS and IIGDM, taking *deeper* gradients by considering U-Net Jacobians is often beneficial for reconstruction performance. Moreover, it even provides way to impose data consistency for non-linear inverse problems, where standard gradient methods are not feasible. In order to devise an analogous method, we take inspiration from DPS, and propose to augment the solver with a gradient step that maximizes the time-dependent likelihood (w.r.t. the measurement) $p(\mathbf{y}|\mathbf{x}_t)$. Specifically, we use the Jensen approximation from [5]

$$\begin{aligned} p(\mathbf{y}|\mathbf{x}_t) &= \int p(\mathbf{y}|\mathbf{x}_0)p(\mathbf{x}_0|\mathbf{x}_t) d\mathbf{x}_0 \\ &= \mathbb{E}_{p(\mathbf{x}_0|\mathbf{x}_t)}[p(\mathbf{y}|\mathbf{x}_0)] \simeq p(\mathbf{y}|\mathbb{E}[\mathbf{x}_0|\mathbf{x}_t]) = p(\mathbf{y}|\hat{\mathbf{x}}_{0|t}), \end{aligned} \quad (15)$$

where the last equality is naturally satisfied from the training objective (9). Using the approximation used in (15), the correcting step under the Gaussian measurement model yields

$$\nabla_{\mathbf{x}_t} \log p(\mathbf{y}|\mathbf{x}_t) \simeq \nabla_{\mathbf{x}_t} \|\mathbf{y} - \mathbf{A} \hat{\mathbf{x}}_{0|t}\|_2^2. \quad (16)$$

Implementing (16) in the place of the shallow gradient update step of Algorithm 1, we achieve CDDDB-deep (see Algorithm 2). From our initial experiments, we find that preconditioning with \mathbf{A}^\dagger as in IIGDM improves performance by a small margin, and hence use this setting as default.

4 Experiments

4.1 Setup

Model, Dataset For a representative DDB, we choose I²SB [26] along with the pre-trained model weights for the following reasons: 1) it is open-sourced⁴, 2) it stands as the current state-of-the-art, 3) the model architecture is based on ADM [11], which induces fair comparison against other DIS methods. All experiments are based on ImageNet 256×256 [10], a benchmark that is considered to be much more challenging for inverse problem solving based on generative models [5], compared to more focused datasets such as FFHQ [20]. We follow the standards of [26] and test our method on the following degradations: sr4x- $\{\text{bicubic, pool}\}$, deblur- $\{\text{uniform, gauss}\}$, and JPEG restoration with 1k validation images.

⁴<https://github.com/NVlabs/I2SB>

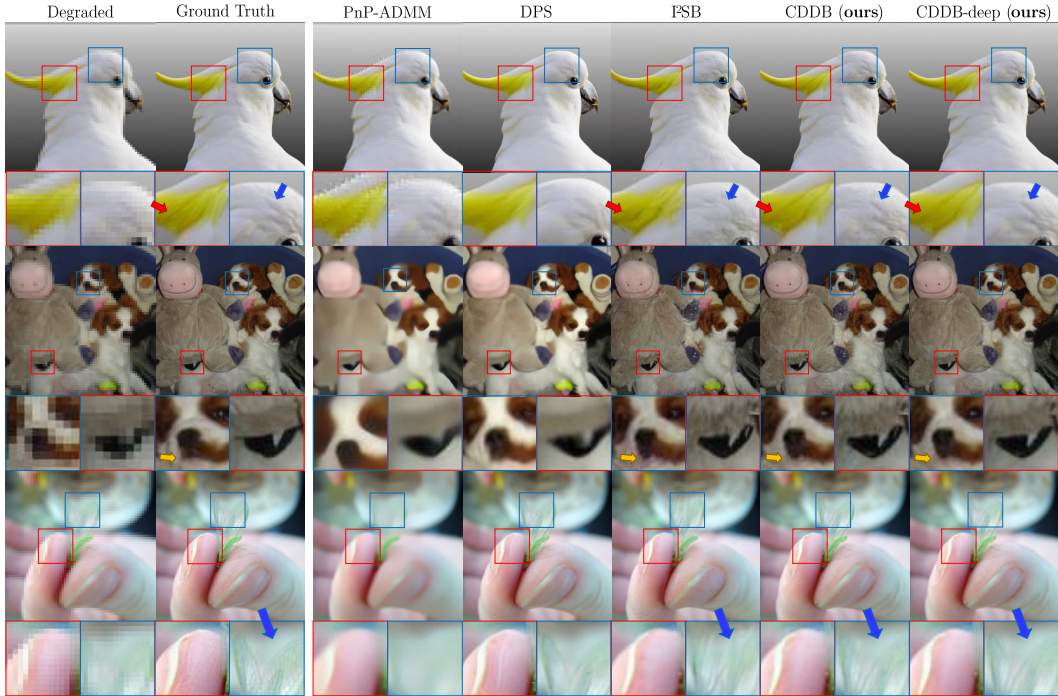


Figure 2: SR($\times 4$)-bicubic reconstruction results. CDDB/CDDB-deep corrects details wrongly captured in I²SB: line texture in 1st row, color/texture errors in 2nd row, topology of wings in 3rd row (see arrows).

Method	SR($\times 4$)								Deblur							
	bicubic				pool				gauss				uniform			
	PSNR \uparrow	SSIM \uparrow	LPIPS \downarrow	FID \downarrow	PSNR \uparrow	SSIM \uparrow	LPIPS \downarrow	FID \downarrow	PSNR \uparrow	SSIM \uparrow	LPIPS \downarrow	FID \downarrow	PSNR \uparrow	SSIM \uparrow	LPIPS \downarrow	FID \downarrow
CDDB (ours)	26.41	0.860	0.198	19.88	<u>26.36</u>	0.855	0.184	17.79	37.02	0.978	0.059	<u>5.007</u>	31.26	0.927	0.193	<u>23.15</u>
I ² SB [26]	25.22	0.802	0.260	24.13	25.08	0.800	0.258	<u>23.53</u>	36.01	0.973	0.067	5.800	<u>30.75</u>	0.919	0.198	23.01
DPS [5]	19.89	0.498	0.384	63.37	21.01	0.562	0.326	49.34	27.21	0.766	0.244	34.58	22.51	0.565	0.357	60.00
IIGDM [36]	<u>26.20</u>	<u>0.850</u>	<u>0.252</u>	29.36	26.07	<u>0.849</u>	<u>0.256</u>	26.97	-	-	-	-	-	-	-	-
DDRM [21]	26.05	0.838	0.270	46.49	25.54	0.848	0.257	40.40	<u>36.73</u>	<u>0.975</u>	0.071	4.346	29.21	0.901	0.210	19.97
DDNM [40]	26.41	0.801	0.230	38.63	26.04	0.792	0.218	33.15	-	-	-	-	-	-	-	-
DDS [6]	26.41	0.801	0.230	38.64	26.04	0.792	0.218	33.15	33.27	0.945	<u>0.057</u>	6.442	27.88	0.829	0.193	26.07
PnP-ADMM [4]	26.16	0.788	0.350	74.06	25.85	0.733	0.372	72.63	28.18	0.800	0.325	60.27	25.47	0.701	0.416	83.76
ADMM-TV	22.55	0.595	0.493	122.7	22.31	0.574	0.512	119.4	24.67	0.773	0.324	50.74	21.72	0.600	0.491	98.15

Table 2: Quantitative evaluation of SR, deblur task on ImageNet 256 \times 256-1k. **Bold**: Best, under: second best. Colored: DDB methods.

Baselines, Evaluation Along with the most important comparison against I²SB, we also include comparisons with state-of-the-art DIS methods including DDRM [21], DPS [5], IIGDM [36], DDNM [40], and DDS [6]. For choosing the NFE and the hyper-parameters for each method, we closely abide to the original advised implementation: DDRM (20 NFE), DPS (1000 NFE), IIGDM (100 NFE), DDNM (100 NFE), DDS (100 NFE). We find that increasing the NFE for methods other than DPS does not induce performance gain. We also note that we exclude IIGDM and DDNM for the baseline comparison in the deblurring problem, as directly leveraging the pseudo-inverse matrix may result in unfair boost in performance [29]. We additionally perform comparisons against PnP-ADMM [4] and ADMM-TV, which are methods tailored towards higher SNR. For I²SB along with the proposed method, we choose 100 NFE for JPEG restoration as we found it to be the most stable, and choose 1000 NFE for all other tasks. Further details on the experimental setup can be found in Appendix C.

4.2 Results

Comparison against baselines Throughout the experiments, we thoroughly analyze both distortion and perception of the reconstructions obtained through our method against other DDB, DIS, and iterative optimization methods. Note that for the recent diffusion-based methods, analysis has been

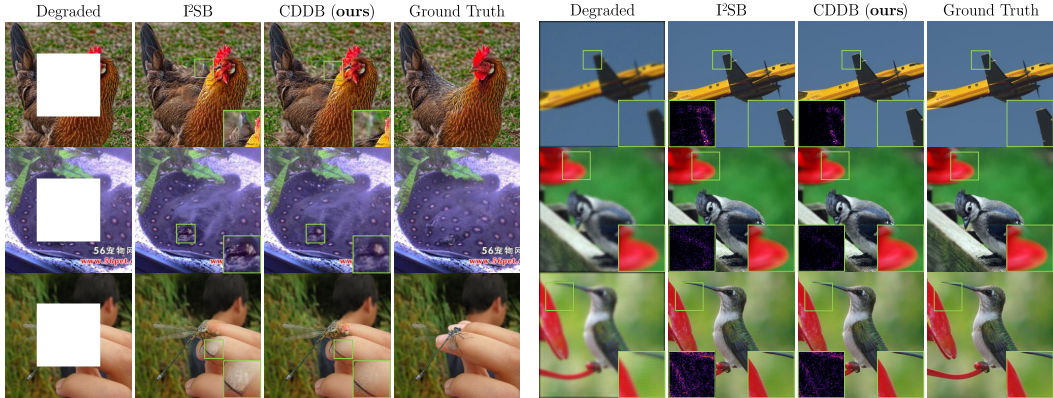


Figure 3: Results on inpainting (Left) and deblurring (Right). For inpainting, boundaries are corrected (row 1) and artifacts are corrected/removed (row 2,3). For deblurring, halo artifacts are corrected, and grid patterns from the background are alleviated.

mainly focused on perceptual metrics [5, 36, 26], mainly because these methods excel on these metrics, but often compromising distortion metrics. DDB methods often take this to the extreme, where one can achieve the best PSNR with very little NFE, and the PSNR consistently degrades as one increases the NFE [9, 26] (See Fig. 1c). Despite this fact, the standard setting in DDB methods is to set a high NFE as one can achieve much improved perceptual quality. On the other hand, conventional iterative methods are often highly optimized for less distortion, albeit with low perceptual quality. While this trade-off may seem imperative, we show that CDDB can improve both aspects, putting it in the place of the state-of-the-art on most experiments (See Tab. 2, 3). A similar trend can be observed in Fig. 2, where we see that CDDB greatly improves the performance of DDB, while also outperforming DIS and iterative optimization methods.

CDDB pushes forward the Pareto-frontier It is widely known that there exists an inevitable trade-off of distortion when aiming for higher perceptual quality [3, 24]. This phenomenon has been reconfirmed consistently in the recent DIS [5, 36] and DDS [9, 26] methods. For DDB, one can flexibly control this trade-off by simply choosing different NFE values, creating a Pareto-frontier with higher NFE tailored towards perceptual quality. While this property is intriguing, the gain we achieve when increasing the NFE decreases *exponentially*, and eventually reaches a bound when $NFE > 1000$. In contrast, we show in Fig. 1 that CDDB pushes the bound further towards the optima. Specifically, 20 NFE CDDB *outperforms* 1000 NFE DDB in PSNR by > 2 db, while having lower FID (i.e. better perceptual quality). To this point, CDDB induces dramatic acceleration ($> 50\times$) to DDB.

Method	PSNR \uparrow	SSIM \uparrow	LPIPS \downarrow	FID \downarrow
CDDB (ours)	26.34	0.837	0.263	19.48
I ² SB [26]	26.12	0.832	0.266	20.35
IIGDM [36]	26.09	0.842	0.282	30.27
DDRM [21]	26.33	0.829	0.330	47.02

Table 3: Quantitative evaluation of the JPEG restoration (QF = 10) task.

CDDB vs. CDDB-deep The two algorithms presented in this work share the same spirit but have different advantages. CDDB generally has higher speed and stability, possibly due to guaranteed convergence. As a result, it robustly increases the performance of SR and deblurring. In contrast, considering the case of inpainting and JPEG restoration, CDDB cannot improve the performance of DDB. For inpainting, the default setting of I²SB ensures consistency by iteratively applying replacement, as implemented in [40]. As the measurement stays in the pixel space, the gradients cannot impose any constraint on the missing pixel values. CDDB-deep is useful in such a situation, as the U-Net Jacobian has a global effect on *all* the pixels, improv-

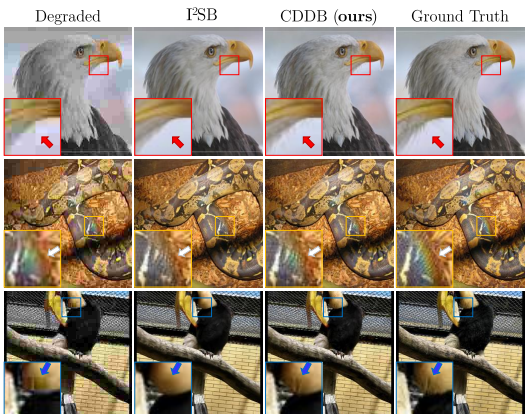


Figure 4: Results on JPEG restoration (QF=10). CDDB recovers texture details (row 1,3), and color details (row 2).

ing the performance by inducing coherence. CDDB-deep also enables the extension to nonlinear inverse problems where one cannot take standard gradient steps. This is illustrated for the case of JPEG restoration in Tab. 3 and Fig. 4, where we see overall improvement in performance compared to I^2SB .

Noise robustness DIS methods are often designed such that they are robust to measurement noise [21, 5]. In contrast, this is not the case for DDB as they are trained in a supervised fashion: If not explicitly trained with synthetic adding of noise, the method does not generalize well to noisy measurements, as can be seen in Fig. 5. On the other hand, note that with CDDB, we are essentially incorporating a Gaussian likelihood model, which naturally enhances the robustness to noise. As a result, while I^2SB tends to propagate noise (best seen in the background), we do not observe such artifacts when using CDDB.

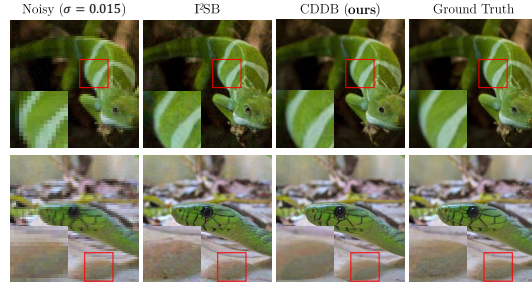


Figure 5: Results on noisy $SR \times 4$ reconstruction. I^2SB propagates noise to the reconstruction. CDDB effectively removes noise.

5 Discussion

Extension to other related works Going beyond the paired inverse problem setting and considering the Schrödinger Bridge (SB) problem [25, 8], or more generally transport mapping problems [27] between the two unmatched distributions, it is often desirable to control the deviation from the start of sampling. A concrete example would be the case of image-to-image translation [43] where one does not want to alter the content of the image. As CDDB can be thought of as a regularization method that penalizes the deviation from the starting point, the application is general and can be extended to such SB problems at inference time by using the gradients that minimize the distance from the start point. We leave this direction for future work.

Data consistency in supervised learning frameworks The first applications of supervised deep learning to solve inverse problems in medical imaging (e.g. CT [17], MRI reconstruction [39]) mostly involved directly inverting the measurement signal without considering the measurement constraints. The works that followed [1, 14] naturally extended the algorithms by incorporating measurement consistency steps in between the forward passes through the neural network. Analogously, CDDB is a natural extension of DDB but with high flexibility, as we do not have to pre-determine the number of forward passes [1] or modify the training algorithm [14].

6 Conclusion

In this work, we unify the seemingly different algorithms under the class of direct diffusion bridges (DDB) and identify the crucial missing part of the current methods: data consistency. Our train-free modified inference procedure named consistent DDB (CDDB) fixes this problem by incorporating consistency-imposing gradient steps in between the reverse diffusion steps, analogous to the recent DIS methods. We show that CDDB can be seen as a generalization of representative DIS methods (DDS, DPS) in the DDB framework. We validate the superiority of our method with extensive experiments on diverse inverse problems, achieving state-of-the-art sample quality in both distortion and perception. Consequently, we show that CDDB can push the Pareto-frontier of the reconstruction toward the desired optimum.

Limitations and societal impact The proposed method assumes prior knowledge of the forward operator. While we limit our scope to non-blind inverse problems, the extension of CDDB to blind inverse problems [7, 30] will be a possible direction of research. Moreover, for certain inverse problems (e.g. inpainting), even when do observe improvements in qualitative results, the quantitative metrics tend to slightly decrease overall. Finally, inheriting from DDS/DIS methods, our method relies on strong priors that are learned from the training data distribution. This may potentially lead to reconstructions that intensify social bias and should be considered in practice.

Acknowledgments and Disclosure of Funding

This research was supported by the KAIST Key Research Institute (Interdisciplinary Research Group) Project, by the National Research Foundation of Korea under Grant NRF-2020R1A2B5B03001980, by the Korea Medical Device Development Fund grant funded by the Korea government (the Ministry of Science and ICT, the Ministry of Trade, Industry and Energy, the Ministry of Health & Welfare, the Ministry of Food and Drug Safety) (Project Number: 1711137899, KMDF_PR_20200901_0015), by Institute of Information & communications Technology Planning & Evaluation (IITP) grant funded by the Korea government(MSIT) (No.2019-0-00075, Artificial Intelligence Graduate School Program(KAIST)), and by the Field-oriented Technology Development Project for Customs Administration through National Research Foundation of Korea(NRF) funded by the Ministry of Science & ICT and Korea Customs Service(NRF-2021M311A1097938).

References

- [1] Hemant K Aggarwal, Merry P Mani, and Mathews Jacob. MoDL: Model-based deep learning architecture for inverse problems. *IEEE transactions on medical imaging*, 38(2):394–405, 2018.
- [2] Thilo Balke, Fernando Davis, Cristina Garcia-Cardona, Michael McCann, Luke Pfister, and Brendt Wohlberg. Scientific Computational Imaging COde (SCICO). Software library available from <https://github.com/lanl/scico>, 2022.
- [3] Yochai Blau and Tomer Michaeli. The perception-distortion tradeoff. In *Proceedings of the IEEE conference on computer vision and pattern recognition*, pages 6228–6237, 2018.
- [4] Stanley H Chan, Xiran Wang, and Omar A Elgendy. Plug-and-play ADMM for image restoration: Fixed-point convergence and applications. *IEEE Transactions on Computational Imaging*, 3(1):84–98, 2016.
- [5] Hyungjin Chung, Jeongsol Kim, Michael Thompson Mccann, Marc Louis Klasky, and Jong Chul Ye. Diffusion posterior sampling for general noisy inverse problems. In *International Conference on Learning Representations*, 2023.
- [6] Hyungjin Chung, Suhyeon Lee, and Jong Chul Ye. Fast diffusion sampler for inverse problems by geometric decomposition. *arXiv preprint arXiv:2303.05754*, 2023.
- [7] Hyungjin Chung, Dohoon Ryu, Michael T Mccann, Marc L Klasky, and Jong Chul Ye. Solving 3d inverse problems using pre-trained 2d diffusion models. *IEEE/CVF Conference on Computer Vision and Pattern Recognition*, 2023.
- [8] Valentin De Bortoli, James Thornton, Jeremy Heng, and Arnaud Doucet. Diffusion schrödinger bridge with applications to score-based generative modeling. *Advances in Neural Information Processing Systems*, 34:17695–17709, 2021.
- [9] Mauricio Delbracio and Peyman Milanfar. Inversion by direct iteration: An alternative to denoising diffusion for image restoration. *arXiv preprint arXiv:2303.11435*, 2023.
- [10] Jia Deng, Wei Dong, Richard Socher, Li-Jia Li, Kai Li, and Li Fei-Fei. Imagenet: A large-scale hierarchical image database. In *2009 IEEE conference on computer vision and pattern recognition*, pages 248–255. Ieee, 2009.
- [11] Prafulla Dhariwal and Alexander Quinn Nichol. Diffusion models beat GANs on image synthesis. In A. Beygelzimer, Y. Dauphin, P. Liang, and J. Wortman Vaughan, editors, *Advances in Neural Information Processing Systems*, 2021.
- [12] Yilun Du, Conor Durkan, Robin Strudel, Joshua B Tenenbaum, Sander Dieleman, Rob Fergus, Jascha Sohl-Dickstein, Arnaud Doucet, and Will Grathwohl. Reduce, reuse, recycle: Compositional generation with energy-based diffusion models and mcmc. In *International conference on machine learning*. PMLR, 2023.
- [13] Bradley Efron. Tweedie’s formula and selection bias. *Journal of the American Statistical Association*, 106(496):1602–1614, 2011.
- [14] Harshit Gupta, Kyong Hwan Jin, Ha Q Nguyen, Michael T McCann, and Michael Unser. Cnn-based projected gradient descent for consistent ct image reconstruction. *IEEE transactions on medical imaging*, 37(6):1440–1453, 2018.

- [15] Jonathan Ho, Ajay Jain, and Pieter Abbeel. Denoising diffusion probabilistic models. *Advances in Neural Information Processing Systems*, 33:6840–6851, 2020.
- [16] Aapo Hyvärinen and Peter Dayan. Estimation of non-normalized statistical models by score matching. *Journal of Machine Learning Research*, 6(4), 2005.
- [17] Kyong Hwan Jin, Michael T McCann, Emmanuel Froustey, and Michael Unser. Deep convolutional network for inverse problems in imaging. *IEEE Transactions on Image Processing*, 26(9):4509–4522, 2017.
- [18] Zahra Kadkhodaie and Eero P Simoncelli. Stochastic solutions for linear inverse problems using the prior implicit in a denoiser. In A. Beygelzimer, Y. Dauphin, P. Liang, and J. Wortman Vaughan, editors, *Advances in Neural Information Processing Systems*, 2021.
- [19] Tero Karras, Miika Aittala, Timo Aila, and Samuli Laine. Elucidating the design space of diffusion-based generative models. In *Proc. NeurIPS*, 2022.
- [20] Tero Karras, Samuli Laine, and Timo Aila. A style-based generator architecture for generative adversarial networks. In *Proceedings of the IEEE/CVF Conference on Computer Vision and Pattern Recognition*, pages 4401–4410, 2019.
- [21] Bahjat Kawar, Michael Elad, Stefano Ermon, and Jiaming Song. Denoising diffusion restoration models. In Alice H. Oh, Alekh Agarwal, Danielle Belgrave, and Kyunghyun Cho, editors, *Advances in Neural Information Processing Systems*, 2022.
- [22] Diederik P Kingma, Tim Salimans, Ben Poole, and Jonathan Ho. Variational diffusion models. *arXiv preprint arXiv:2107.00630*, 2021.
- [23] Ken Kreutz-Delgado. The complex gradient operator and the cr-calculus. *arXiv preprint arXiv:0906.4835*, 2009.
- [24] Christian Ledig, Lucas Theis, Ferenc Huszár, Jose Caballero, Andrew Cunningham, Alejandro Acosta, Andrew Aitken, Alykhan Tejani, Johannes Totz, Zehan Wang, et al. Photo-realistic single image super-resolution using a generative adversarial network. In *Proceedings of the IEEE conference on computer vision and pattern recognition*, pages 4681–4690, 2017.
- [25] Christian Léonard. A survey of the schrödinger problem and some of its connections with optimal transport. *arXiv preprint arXiv:1308.0215*, 2013.
- [26] Guan-Hong Liu, Arash Vahdat, De-An Huang, Evangelos A Theodorou, Weili Nie, and Anima Anandkumar. I²SB: Image-to-Image Schrödinger Bridge. In *International conference on machine learning*. PMLR, 2023.
- [27] Xingchao Liu, Chengyue Gong, and qiang liu. Flow straight and fast: Learning to generate and transfer data with rectified flow. In *The Eleventh International Conference on Learning Representations*, 2023.
- [28] Ziwei Luo, Fredrik K Gustafsson, Zheng Zhao, Jens Sjölund, and Thomas B Schön. Image restoration with mean-reverting stochastic differential equations. In *International conference on machine learning*. PMLR, 2023.
- [29] Sladjana Miljković, Marko Miladinović, Predrag Stanimirović, and Igor Stojanović. Application of the pseudoinverse computation in reconstruction of blurred images. *Filomat*, 26(3):453–465, 2012.
- [30] Naoki Murata, Koichi Saito, Chieh-Hsin Lai, Yuhta Takida, Toshimitsu Uesaka, Yuki Mitsufuji, and Stefano Ermon. Gibbsddrm: A partially collapsed gibbs sampler for solving blind inverse problems with denoising diffusion restoration. In *International conference on machine learning*. PMLR, 2023.
- [31] Aditya Ramesh, Prafulla Dhariwal, Alex Nichol, Casey Chu, and Mark Chen. Hierarchical text-conditional image generation with clip latents. *arXiv preprint arXiv:2204.06125*, 2022.
- [32] Robin Rombach, Andreas Blattmann, Dominik Lorenz, Patrick Esser, and Björn Ommer. High-resolution image synthesis with latent diffusion models. In *Proceedings of the IEEE/CVF Conference on Computer Vision and Pattern Recognition*, pages 10684–10695, 2022.
- [33] Chitwan Saharia, William Chan, Saurabh Saxena, Lala Li, Jay Whang, Emily L Denton, Kamyar Ghasemipour, Raphael Gontijo Lopes, Burcu Karagol Ayan, Tim Salimans, et al. Photorealistic text-to-image diffusion models with deep language understanding. *Advances in Neural Information Processing Systems*, 35:36479–36494, 2022.

- [34] Tim Salimans and Jonathan Ho. Should ebms model the energy or the score? In *Energy Based Models Workshop-ICLR 2021*, 2021.
- [35] Jiaming Song, Chenlin Meng, and Stefano Ermon. Denoising diffusion implicit models. In *9th International Conference on Learning Representations, ICLR*, 2021.
- [36] Jiaming Song, Arash Vahdat, Morteza Mardani, and Jan Kautz. Pseudoinverse-guided diffusion models for inverse problems. In *International Conference on Learning Representations*, 2023.
- [37] Yang Song and Stefano Ermon. Generative modeling by estimating gradients of the data distribution. In *Advances in Neural Information Processing Systems*, volume 32, 2019.
- [38] Yang Song, Jascha Sohl-Dickstein, Diederik P. Kingma, Abhishek Kumar, Stefano Ermon, and Ben Poole. Score-based generative modeling through stochastic differential equations. In *9th International Conference on Learning Representations, ICLR*, 2021.
- [39] Shanshan Wang, Zhenghang Su, Leslie Ying, Xi Peng, Shun Zhu, Feng Liang, Dagan Feng, and Dong Liang. Accelerating magnetic resonance imaging via deep learning. In *2016 IEEE 13th international symposium on biomedical imaging (ISBI)*, pages 514–517. IEEE, 2016.
- [40] Yinhuai Wang, Jiwen Yu, and Jian Zhang. Zero-shot image restoration using denoising diffusion null-space model. In *The Eleventh International Conference on Learning Representations*, 2023.
- [41] Jong Chul Ye. *Geometry of Deep Learning*. Springer, 2022.
- [42] Kai Zhang, Wangmeng Zuo, Yunjin Chen, Deyu Meng, and Lei Zhang. Beyond a gaussian denoiser: Residual learning of deep CNN for image denoising. *IEEE transactions on image processing*, 26(7):3142–3155, 2017.
- [43] Jun-Yan Zhu, Taesung Park, Phillip Isola, and Alexei A Efros. Unpaired image-to-image translation using cycle-consistent adversarial networks. In *Proceedings of the IEEE international conference on computer vision*, pages 2223–2232, 2017.

A Proofs

Theorem 1. Let the parameters of InDI [9] in Table 1 be $t := \frac{\gamma_t^2}{\gamma_t^2 + \bar{\gamma}_t^2}$, $\epsilon_t^2 := \frac{\bar{\gamma}_t^2}{\gamma_t^2}(\gamma_t^2 + \bar{\gamma}_t^2)$. Then, InDI and I²SB are equivalent.

Proof. In order to proceed with the proof, we first remind the notations from Table 1:

$$\gamma_t^2 := \int_0^t \beta_\tau d\tau, \quad \bar{\gamma}_t^2 := \int_t^1 \beta_\tau d\tau. \quad (17)$$

By definition, we note that $\gamma_t^2 + \bar{\gamma}_t^2 = \int_0^1 \beta_\tau d\tau$ is constant for any choice of $t \in [0, 1]$. To proceed with the proof, we have for $\alpha_{s|t}^2$,

$$s/t = \frac{\gamma_s^2}{\gamma_s^2 + \bar{\gamma}_s^2} / \frac{\gamma_t^2}{\gamma_t^2 + \bar{\gamma}_t^2} = \frac{\gamma_s^2}{\gamma_t^2}. \quad (18)$$

Considering $\sigma_{s|t}^2$,

$$s^2(\epsilon_s^2 - \epsilon_t^2) = \frac{\gamma_s^4}{(\gamma_s^2 + \bar{\gamma}_s^2)^2} \left(\frac{\bar{\gamma}_s^2}{\gamma_s^2}(\gamma_s^2 + \bar{\gamma}_s^2) - \frac{\bar{\gamma}_t^2}{\gamma_t^2}(\gamma_t^2 + \bar{\gamma}_t^2) \right) \quad (19)$$

$$= \frac{\gamma_s^4}{\gamma_s^2 + \bar{\gamma}_s^2} \left(\frac{\bar{\gamma}_s^2}{\gamma_s^2} - \frac{\bar{\gamma}_t^2}{\gamma_t^2} \right) \quad (20)$$

$$= \frac{\gamma_s^2}{\gamma_s^2 + \bar{\gamma}_s^2} \left(\frac{\bar{\gamma}_s^2 \gamma_t^2 - \bar{\gamma}_t^2 \gamma_s^2}{\gamma_t^2} \right) \quad (21)$$

$$\stackrel{(a)}{=} \frac{\gamma_s^2}{\gamma_s^2 + \bar{\gamma}_s^2} \frac{d_s^2(\gamma_t^2 + \bar{\gamma}_t^2)}{\gamma_t^2} \quad (22)$$

$$= \frac{\gamma_s^2}{\gamma_t^2} d_s^2 \quad (23)$$

$$= \frac{\gamma_s^2}{\gamma_t^2} (\gamma_t^2 - \gamma_s^2), \quad (24)$$

where in (a), we defined $d_s^2 := \int_s^t \beta_\tau d\tau$ such that $\gamma_s^2 + d_s^2 = \gamma_t^2$ is satisfied. \square

Theorem 2. The total variance condition (12) is satisfied for both I²SB and InDI.

Proof. Here, we further show that the condition is satisfied for I²SB for completeness.

$$\sigma_s^2 - (\alpha_{s|t}^2)^2 \sigma_t^2 = \frac{\gamma_s^2 \bar{\gamma}_s^2}{\gamma_s^2 + \bar{\gamma}_s^2} - \frac{\gamma_s^4}{\gamma_t^4} \frac{\gamma_t^2 \bar{\gamma}_t^2}{\gamma_t^2 + \bar{\gamma}_t^2} \quad (25)$$

$$= \frac{\gamma_s^2}{\gamma_s^2 + \bar{\gamma}_s^2} \left(\bar{\gamma}_s^2 - \frac{\gamma_s^2 \bar{\gamma}_t^2}{\gamma_t^2} \right) \quad (26)$$

$$= \frac{\gamma_s^2}{\gamma_t^2} \frac{\bar{\gamma}_s^2 \gamma_t^2 - \gamma_s^2 \bar{\gamma}_t^2}{\gamma_s^2 + \bar{\gamma}_s^2} \quad (27)$$

$$= \frac{\gamma_s^2}{\gamma_t^2} \frac{(\bar{\gamma}_t^2 + d_s^2) \gamma_t^2 - \gamma_s^2 (\gamma_t^2 - d_s^2)}{\gamma_s^2 + \bar{\gamma}_s^2} \quad (28)$$

$$= \frac{\gamma_s^2}{\gamma_t^2} \frac{d_s^2 (\gamma_t^2 + \bar{\gamma}_t^2)}{\gamma_s^2 + \bar{\gamma}_s^2} \quad (29)$$

$$= \frac{\gamma_s^2 (\gamma_t^2 - \gamma_s^2)}{\gamma_t^2} = \sigma_{s|t}^2, \quad (30)$$

where we use $\gamma_s^2 + d_s^2 = \gamma_t^2$ for the last equality. \square

B Details on Table 1

I²SB $\beta_{\min} = 0.0001$, $\beta_{\max} = 0.02$. The same β_t schedule is used regardless of being implemented as deterministic or not. For the former, $\sigma_t = \sigma_{s|t}^2 = 0$.

InDI The speed of the base degradation process is parametrized with constant time-speed t . For deterministic methods, $\epsilon_t = 0$ and hence $\sigma_t = \sigma_{s|t}^2 = 0$. For stochastic methods, $\epsilon_t = 0.01$ such that $\sigma_{s|t}^2 = 0$.

IR-SDE (PF-ODE) As mentioned in the main text, IR-SDE can also be considered a type of DDB as it obeys the marginal distribution that is characterized by (8), but with a different sampling method. Specifically, we can set $\alpha_t = 1 - e^{-\theta t}$, $\sigma_t^2 = \lambda^2(1 - e^{-2\theta t})$, with $\delta = 0.008$. λ^2 is the stationary variance of the OU-process, which is set to the noise variance of the degraded image. For all non-noisy inverse problems that we mostly consider in this work, λ^2 is still set to $10/255$.

C Experimental Details

C.1 Implementation Details

Models All the models that are used throughout the work are based on pre-trained models from I²SB⁵. All the models are fine-tuned from the ADM [11] ImageNet 256×256 model, hence share the same architecture as well as the specific model hyper-parameter settings.

Inverse problem setting All the forward operators \mathbf{A} are used in the same manner as in [26], which are adopted from DDRM [21].

Step size, gradient For both Algorithms 1,2, we use constant step size, but scaled to match the signal ratio of the intermediate reconstructions $\hat{x}_{0|i}$: $\rho_i = (1 - \alpha_{i|i+1}^2)c$, where c is some constant. For SR and deblurring tasks, we take $c = 1.0$. For JPEG restoration, we take $c = 0.5$.

When implementing the gradient computation for CDDB, we do not explicitly compute \mathbf{A}^\top , but rely on automatic differentiation for simplicity. This lets us unify the implementations of Algorithm 1,2 in a similar manner.

Compute All experiments were run using a single RTX 3090 GPU. On average, I²SB and CDDB with 1000 NFE take about 82 seconds (~ 0.08 sec. / iter). CDDB-deep takes about 193 seconds (~ 0.19 sec. / iter).

Code Availability Code is available at <https://github.com/HJ-harry/CDDB>

C.2 Comparison Methods

I²SB We follow the default setting advised in [26] and set the default sampling schedule to be the quadratic schedule [35] with 1000 NFE. As we leverage the pre-trained checkpoints provided, deblurring and inpainting models are set to OT-ODE with no additive Gaussian noise during the sampling process.

DPS, IIGDM Pre-trained ADM models that were used in the original work [5, 36] are used. For DPS, we use the constant step size of 1.0 with 1000 NFE. For IIGDM, we use the constant step size of 1.0 with 100 NFE. We initially experimented with higher NFE for IIGDM but did not find a boost in performance.

DDRM We use 20 NFE DDIM sampling with $\eta = 0.85$, $\eta_b = 1.0$ as advised.

DDNM We use 100 NFE sampling with $\eta = 0.85$ as advised. We do not use time travel for all experiments.

⁵<https://github.com/NVlabs/I2SB>

$c =$	CDDB								CDDB-deep							
	0.0	0.25	0.5	0.75	1.0	1.5	2.0	3.0	0.0	0.25	0.5	0.75	1.0	1.5	2.0	3.0
PSNR (\uparrow)	25.07	26.14	26.28	26.31	26.31	26.30	26.24	25.70	25.07	26.21	26.42	26.51	26.56	26.59	26.57	26.06
SSIM (\uparrow)	0.692	0.744	0.752	0.753	0.753	0.751	0.747	0.729	0.692	0.745	0.756	0.760	0.761	0.762	0.760	0.747
LPIPS (\downarrow)	0.271	0.218	0.206	0.203	0.201	0.202	0.207	0.244	0.271	0.226	0.214	0.209	0.205	0.202	0.202	0.227
FID (\downarrow)	37.78	32.81	30.76	29.89	29.33	28.99	29.85	37.22	37.78	35.07	33.17	32.25	29.29	29.97	29.71	34.22

Table 4: Step size ablation on the step size for CDDB $c := \rho_i / (1 - \alpha_{i|i+1}^2)$ using 100 test images on SR \times 4-bicubic task, NFE=100. **I²SB** [26], **Chosen step size**.

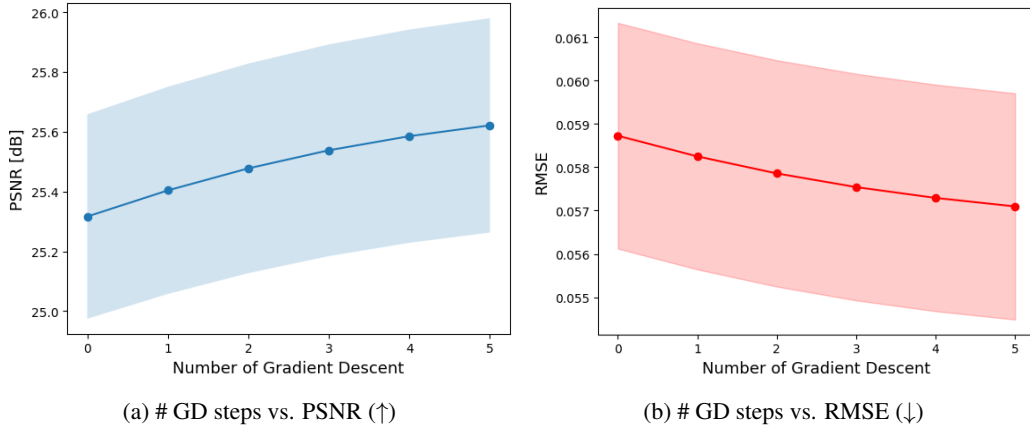


Figure 6: Effect of gradient descent (GD) steps in CDDB applied to intermediate samples $\hat{x}_{0|i}$. Mean ± 0.1 std indicated as colored region.

DDS We use 100 NFE sampling with $\eta = 0.85$ since we did not observe additional performance gain with larger NFE.

PnP-ADMM, ADMM-TV Following [5], we use the implementation provided in the `scico` library [2]. For PnP-ADMM, we use $\rho = 0.2$, `max_iter`=12 with the DnCNN [42] denoiser. For ADMM-TV, we use as the regularization term $\lambda \|\mathbf{D}\mathbf{x}_0\|_{2,1}$ with $(\lambda, \rho) = (2.7e - 2, 1.4e - 1)$ for deblurring and $(\lambda, \rho) = (2.7e - 2, 1.0e - 2)$ for SR.

C.3 Evaluation

Out of the default 10k evaluation images from 256 \times 256 ImageNet [10] used in [26], we use 1k images by interleaved sampling: i.e. Images of index 0, 10, 20, ... are used. When computing the FID score, we use the `pytorch-fid` package and compare the distribution of the ground truth images vs. the reconstructed images, rather than comparing against the training data, following the setting of [5].

D Ablation Studies

D.1 Step size

In Table 4, we summarize the effect of the choice of step size when implementing CDDB/CDDB-deep. Note that for *all* choice of step sizes, the quantitative metrics are superior to the I²SB counterpart, which states that CDDB stably improves the performance. We observe that for both methods, $c = 1.0$ strikes a good balance between the distortion and the perception metrics. For CDDB-deep, taking a slightly larger step size (e.g. $c = 1.5$) improves performance for certain problems, but we keep $c = 1.0$ for unity.

D.2 Effect of gradients during sampling

In Fig. 6, we investigate the effect of the CDDB gradient steps when applied to $\hat{x}_{0|i}$ (i.e. intermediate denoised estimate) with $i = N//2^6$, 10 NFE for 300 test samples on SR \times 4-bicubic task. Note that we can apply multiple GD steps to the intermediate denoised sample $\hat{x}_{0|i}$, which is indicated in the x -axis of the figures. Even when we apply multiple GD steps, we observe that the metrics constantly get better, establishing the stability of the proposed method.

⁶python notation